# 2 Pulsars

• Two more key properties of neutron stars can be identified, connecting them to their observational manifestation, **pulsars**. **C & O, Sec. 16.7**

∗ They rotate rapidly. *Angular momentum conservation* during core collapse establishes $I\Omega$ as a constant of the evolution. Hence, as $I \sim MR^2$ and $\Omega = 2\pi/P$, we expect a period/radius relation as follows:

$$P_{ns} \sim P_{\odot} \left( \frac{R_{\rm ns}}{R_{\odot}} \right)^2 \quad . \tag{12}$$

This leads to periods of $10^{-3}$ seconds!

∗ They possess intense fields. *Magnetic flux conservation* during core collapse yields

$$\Phi = \int_S \vec{B}.d\vec{A} \sim 4\pi R^2 B \tag{13}$$

as a constant of the evolution. Hence we expect

$$B_{ns} \sim B_{\odot} \left( \frac{R_{\odot}}{R_{\rm ns}} \right)^2 \quad , \tag{14}$$

i.e. of the order of $10^{10} - 10^{12}$ Gauss for solar-type fields in the progenitors.

• Pulsars were first observed in 1967 by Hewish and Bell, leading to the Nobel Prize in physics for Hewish. They are mostly *radio* pulsars, with some 2500 observed so far in all wavebands, many in the Parkes multi-beam survey and also precipitated by the Arecibo upgrade.

**Plot:** Pulsar Signal from PSR B1919+21 and Geometry

They exhibit periodic signals, with a period range mostly constrained to

$$\boxed{0.002 \text{ sec} \lesssim P \lesssim 10 \text{ sec}} \tag{15}$$

This period is not constant, but slowly and steadily increases in time, leading to a key observable $\dot{P} \equiv dP/dt$.

# The Pulsar Phenomenon

Spin-powered pulsars: rotating, magnetized neutron stars.

**PSR B1919+21**

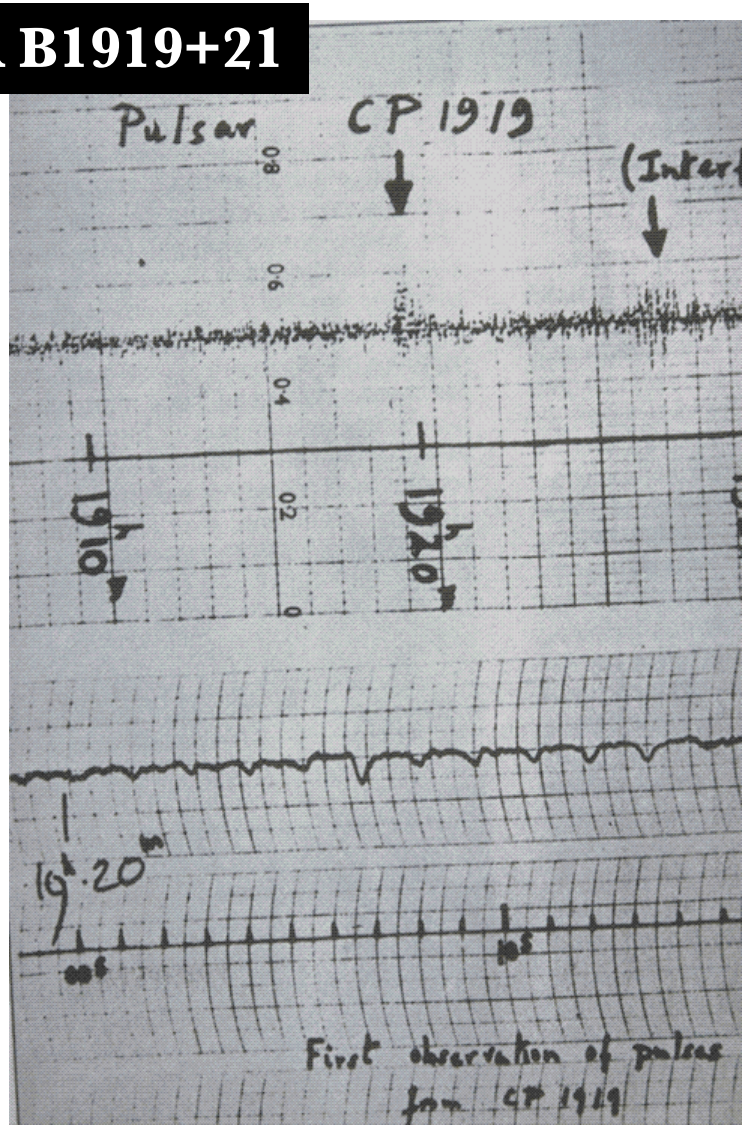


**1967: discovery of pulsars by Jocelyn Bell and Antony Hewish**

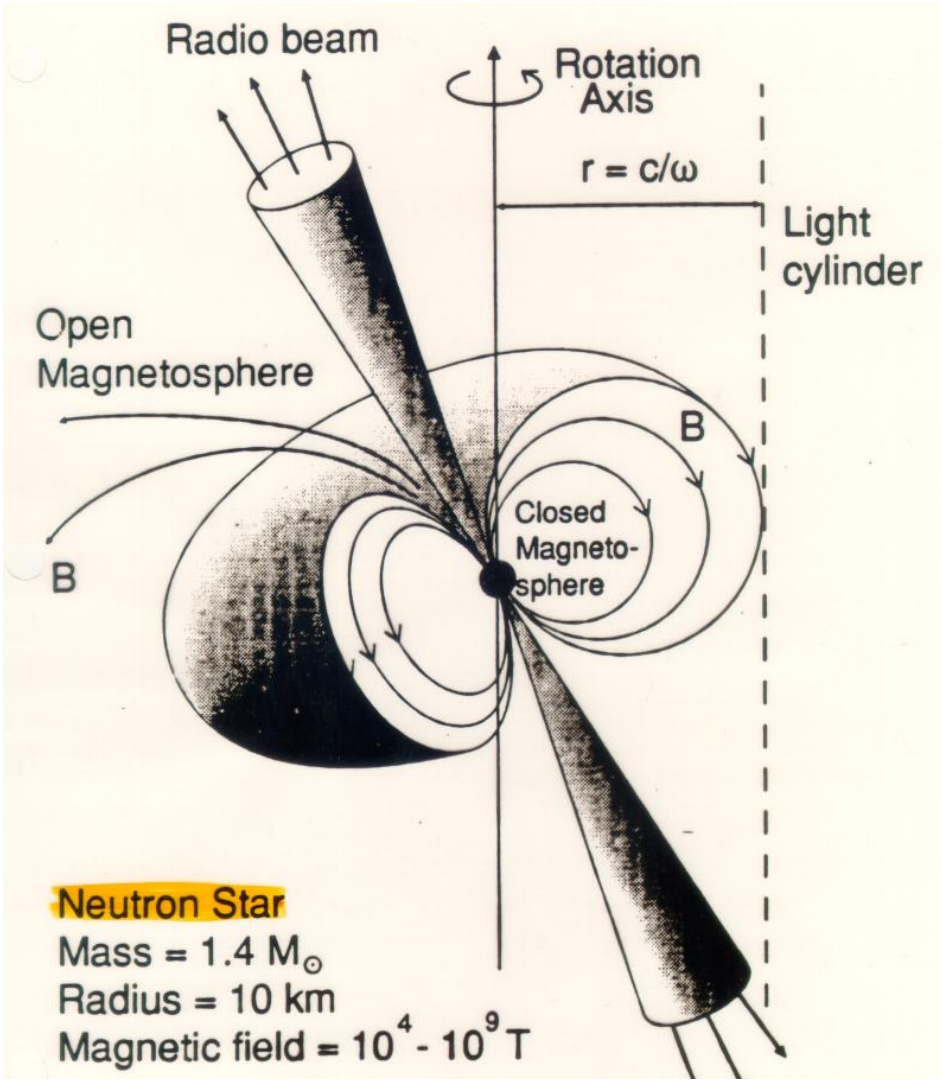


**Typical picture of rotating neutron star.**

***Slide: courtesy of David Thompson***

• There are over 3000 radio pulsars, around 60 X-ray pulsars, and around 30 optical pulsars known to date. The launch of *Fermi* in June 2008 led to the detection of over 300 gamma-ray pulsars (December 2025 count).

Pulsars reside predominantly in or near the galactic plane, the notable exception being **millisecond pulsars** (MSPs) in globular clusters.

**Plot:** Pulsar Sky Distribution circa 2023

---

• Pulsar periods cannot be orbital in character: they are too short, yielding Keplerian orbits of semi-major axis $a \lesssim R_{\rm ns} \ll R_{\rm wd} \ll R_\odot$ .

∗ Binary neutron stars could work, but inspiral due to radiative and gravitational effects would lead to $\dot{P} < 0$ , contrary to observations of $\dot{P} > 0$ in the pulsar majority (exception: episodic spin-up in millisecond pulsars).

∗ Pulsars are not pulsating stars: sound crossing times for white dwarfs yield periods $P \sim 1/\sqrt{G\rho} \sim 10^3$sec $\gg P_{\rm psr}$ , and for neutron stars give $P \sim 1/\sqrt{G\rho} \sim 10^{-4}$sec $\ll P_{\rm psr}$ .

• The *rotating neutron star model for pulsars* is the only viable one, and has become widely accepted. Pulsars cannot spin arbitrarily fast; the centripetal acceleration cannot exceed the gravitational one, otherwise **break-up** will occur. The criterion for rotational stability is therefore

$$(\Omega R)^2 \lesssim \frac{GM}{R} \quad \Rightarrow \quad P \equiv \frac{2\pi}{\Omega} \gtrsim 2\pi \sqrt{\frac{R^3}{GM}} \tag{16}$$

which is just under a millisecond for neutron stars.

• The most luminous band for emission by pulsars is actually gamma rays, and *Fermi*-LAT has detected just over 300 gamma-ray pulsars above 100 MeV in energy. The most powerful of these are the Vela and Crab pulsars, both discovered as radio pulsars in 1968.

**Plot:** Vela Pulsar Light Curve

# The Galactic Pulsar Population

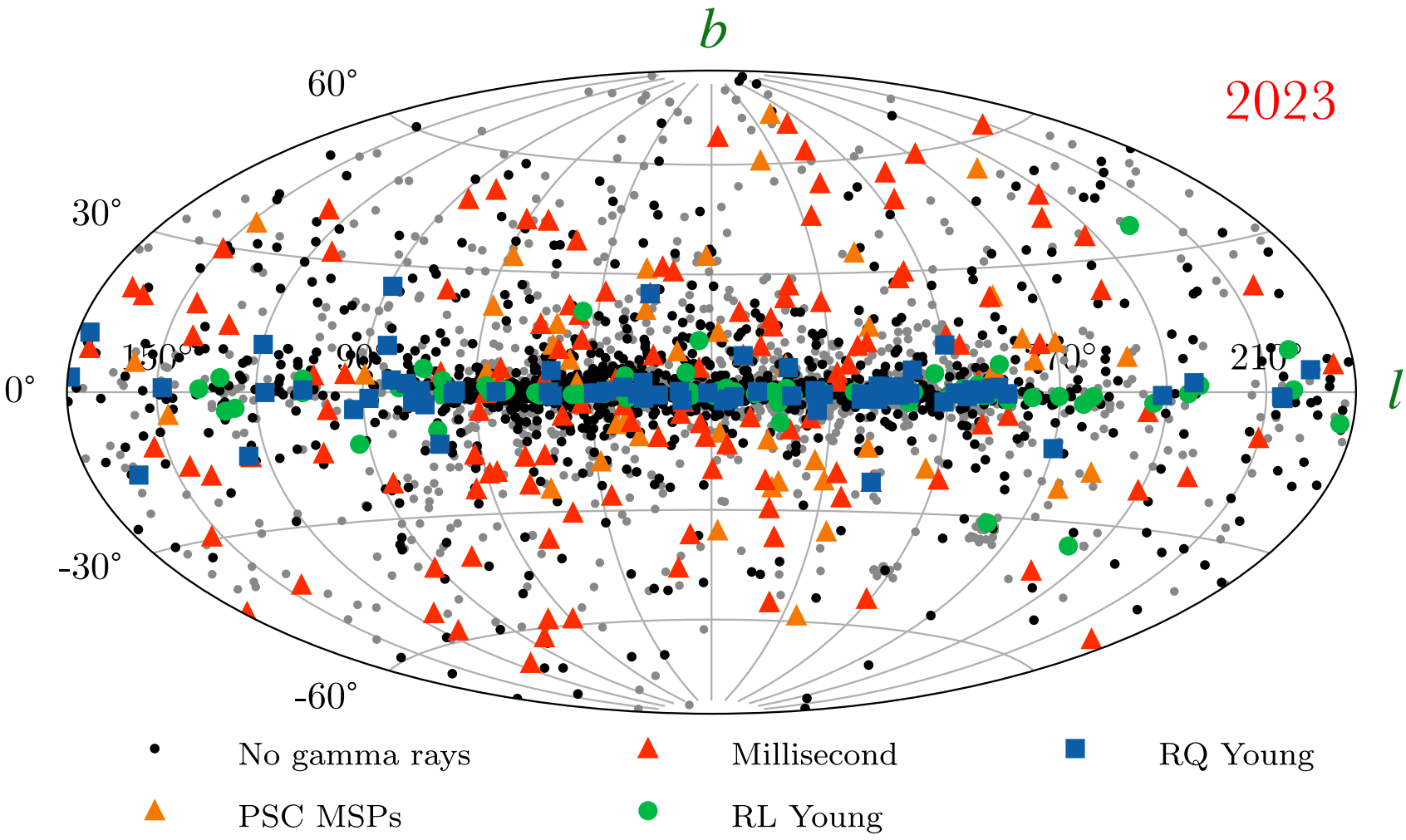


**Figure 3.** Pulsar sky map in Galactic coordinates (Hammer projection). Symbols are the same as in Figure 2.

Third *Fermi* Pulsar Catalog (Smith et al., ApJ **958**:191, 2023)

# Energy-Dependent Pulse Profiles - Vela

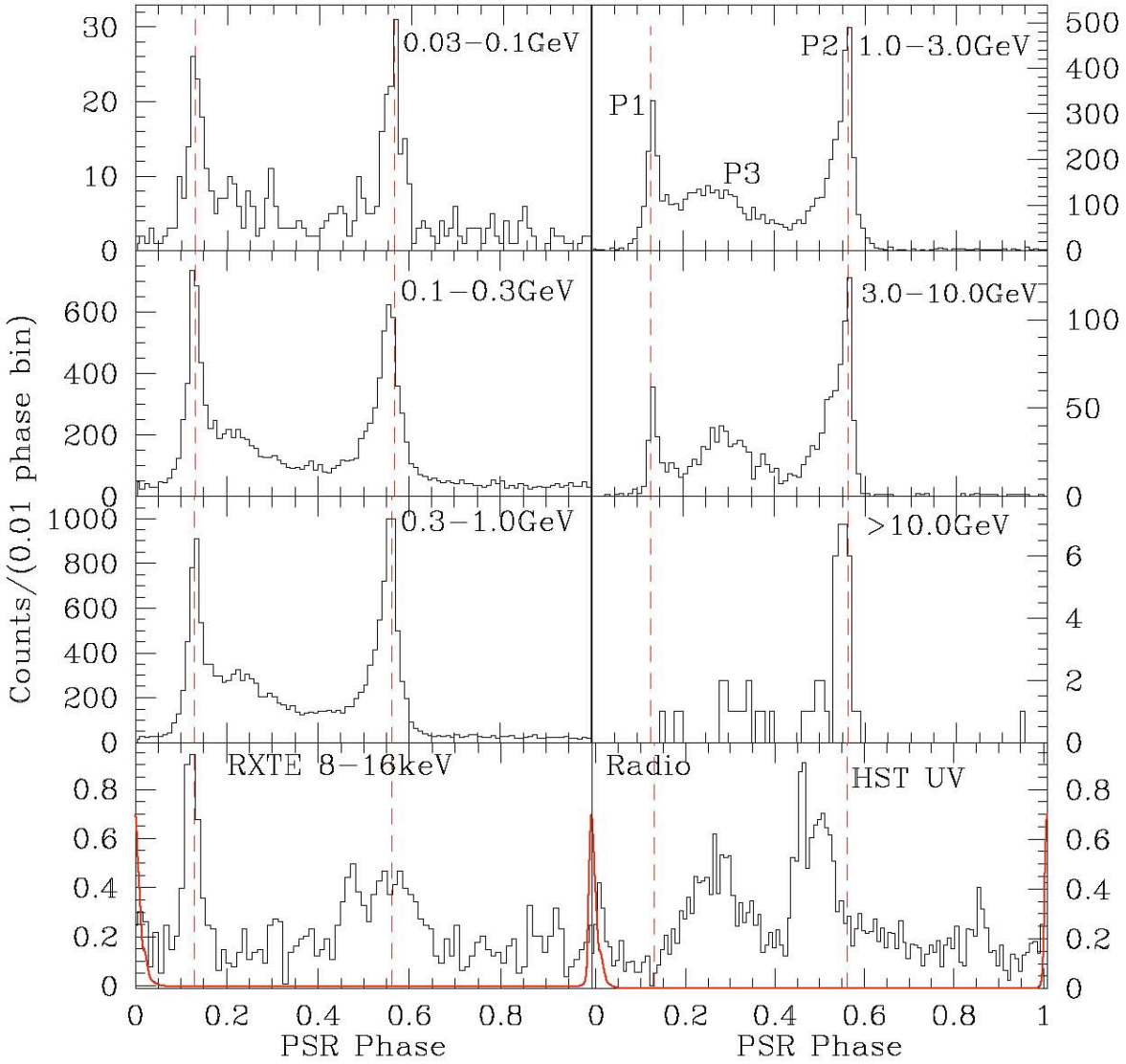


Abdo et al. 2009 ApJ, 696, 1089.

FIG. 2. — The evolution of the Vela $\gamma$-ray pulse profile over three decades of energy. Each pulse profile is binned to 0.01 of pulsar phase, and dashed lines show the phases of the P1 and P2 peaks determined from the broad band light curve. In the top right panel we label the main peaks P1, P2 and P3. In the bottom panels we show at left the 8-16 keV *RXTE* pulse profile of Harding et al. (2002) along with the radio pulse profile (in red). At lower right, the 4.1-6.5 eV *HST*/STIS NUV pulse profile of Romani et al. (2005) is shown for comparison.

## 2.1 Radio Pulse Dispersion

• Pulsar radio signals are dispersed by free electrons in the ISM, and this dispersion is frequency-dependent. High frequency emission ( $\sim 1.4\,\mathrm{GHz}$) arrives slightly before lower frequency light ( $\sim 440\,\mathrm{MHz}$):

**Plot:** Pulse Dispersion from PSR 1641-45

The *energy information or Poynting flux propagates at* the **group velocity**

$$v_g \equiv \frac{d\omega}{dk} = c\left(1-\frac{\omega_p^2}{\omega^2}\right)^{1/2} \approx c\left(1-\frac{\omega_p^2}{2\omega^2}\right) \quad . \tag{17}$$

Herein, $\omega_p^2 = 4\pi\langle n_e\rangle e^2/m_e$ is the square of the **electron plasma frequency** $\omega_p$, and $n \approx 1-\omega_p^2/(2\omega^2)$ is the refractive index. Accordingly, high frequency EM waves arrive from a distant pulsar before ones of lower frequency do. The relative delay compared with waves of infinite frequency (essentially satisfied by gamma-rays) is

$$\Delta t(\omega) = \int_0^d \frac{dl}{v_g} - \frac{d}{c} \approx \frac{1}{c}\int_0^d \frac{\omega_p^2}{2\omega^2}\,dl = \frac{2\pi e^2}{m_e c}\,\frac{DM}{\omega^2} \quad . \tag{18}$$

The line-of-sight value of $\langle n_e\rangle$ forms the **dispersion measure**,

$$DM = \int_0^d n_e\,dl \quad . \tag{19}$$

Thus, $d = DM/\langle n_e\rangle$, and this useful pulsar distance estimate is accurate to the level that the Galactic ISM electron density (heavily influenced by clumped HII regions) can be known, generally around a factor of 2 or so.

The typical scale of the time delays is

$$\Delta t(\omega) = 2.14\left(\frac{\nu}{0.44\,\mathrm{GHz}}\right)^{-2}\left(\frac{n_e}{0.1\,\mathrm{cm}^{-3}}\right)\left(\frac{d}{1\,\mathrm{kpc}}\right)\mathrm{sec} \quad , \tag{20}$$

for fiducial ISM parameters and a representative radio observation frequency $\nu = 2\pi\omega = 440$ MHz. While the net delay generally exceeds the pulse period, what is most relevant is that the relative delay over a small frequency band, for which $\Delta\nu/\nu \ll 1$.

# Pulse Dispersion for PSR 1641-45

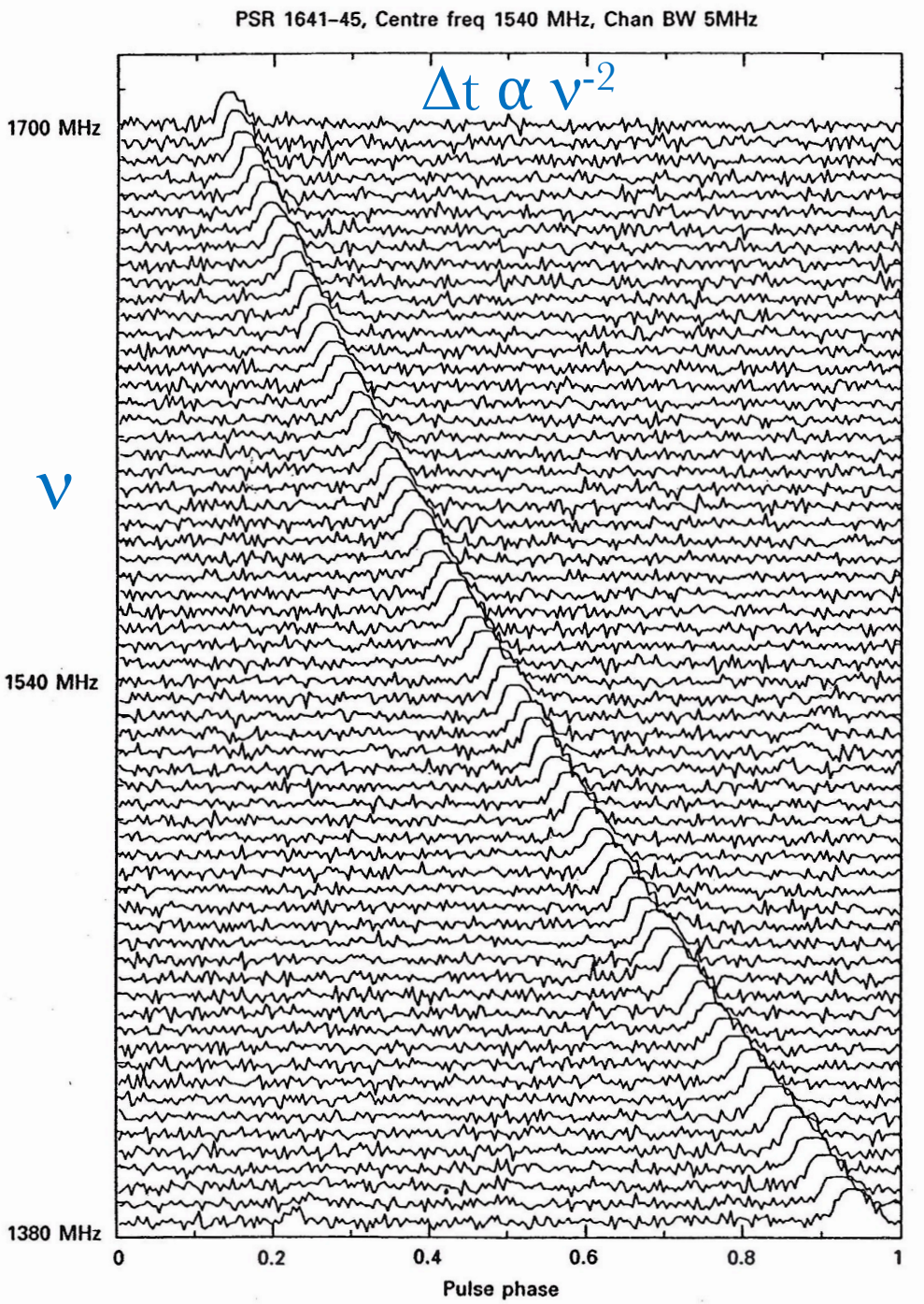


P=0.455sec

- Dispersion of the 1380-1700 MHz pulses for PSR 1641-45. Observe the clean quadratic dependence on $\nu^{-2}$.
- From Lyne & Graham-Smith *Pulsar Astronomy* (1990, Cambridge Univ. Press).

## 2.2 Pulsar Rotational Spin-Down

• Since the quasi-dipolar field structure is generally obliquely oriented with respect to the spin axis (with angle $\alpha \neq 0$), pulsars spin down due to **magnetic dipole radiation** (*vacuum solution*): **C & O, pp. 597-9**

$$\frac{dE}{dt} = -\frac{8\pi^4 B^2 R_{\rm ns}^6 \sin^2\alpha}{3c^3 P^4} \equiv \frac{1}{2}\,\frac{d}{dt}\big(I\Omega^2\big) \tag{21}$$

Here $I \sim 2M_{\rm ns}R_{\rm ns}^2/5 \sim 10^{45}\,{\rm g\ cm^2}$ is the neutron star moment of inertia.

**Plot:** Rotating Dipole Model Geometry

Setting $\Omega = 2\pi/P$, Eq. (21) can be solved for $P(t) \propto t^{1/2}$, and inverted to derive observational inferences for the polar field strength

$$\boxed{B_{\rm p}\sin\alpha \;=\; 6.4\times 10^{19}\,\sqrt{P\,\dot{P}}\ {\rm Gauss}} \tag{22}$$

from pulsar spin characteristics. This is the conventional method for determining pulsar field estimates. Uncertainties pervade it due to the assumed $I$ value (an EOS issue) and non-vacuum contributions to the torque.

**Plot:** $P$-$\dot{P}$ Diagram for Pulsars

• The same solution can be used to define the **characteristic age** or spin-down lifetime for a pulsar:

$$\tau \;=\; \frac{P}{2\dot{P}} \quad . \tag{23}$$

These ages can be compared with expansion/dynamical ages of associated supernova remnants in dozens of cases.

The solution also determines the **spin-down luminosity** $\dot{E} \equiv dE/dt$, which is generally found to be in the range of $10^{32} \lesssim \dot{E} \lesssim 10^{38}\,{\rm erg/sec}$ in the X-ray and gamma-ray wavebands, and somewhat lower in the radio. This element means that the **electromagnetic torque** that extracts angular momentum from the spinning star also extracts energy in the form of coherent **Poynting flux** at a frequency $\Omega/2\pi$ radiated to infinity, along with plasma.

# Rotating dipole model

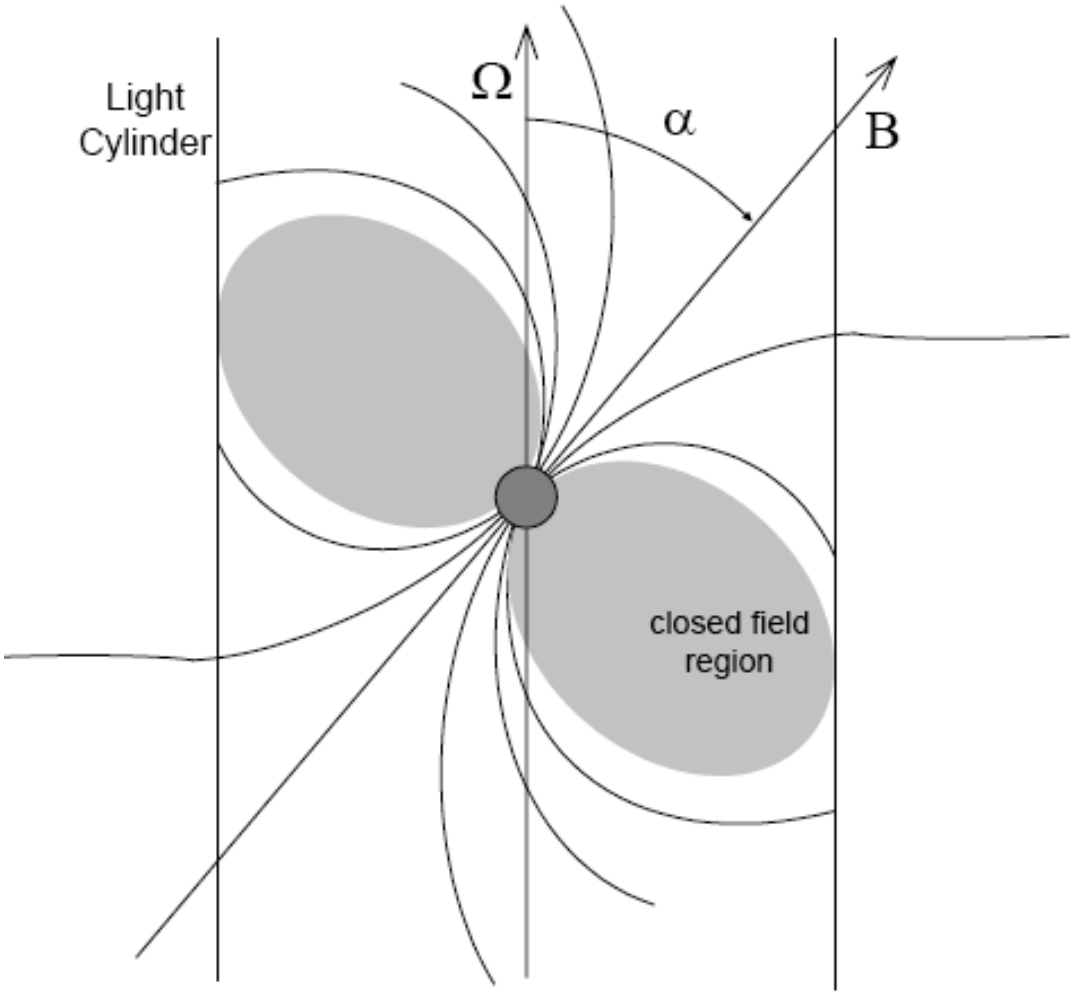


- **Magnetic dipole radiation**

$$\dot{E}_{SD} = -\frac{B_0^2 \sin^2\alpha\, \Omega^4 R^6}{6c^3} = I\Omega\dot{\Omega}$$

- **Braking index**

$$\dot{\Omega} = -K\Omega^n \qquad n = \frac{\ddot{\Omega}\Omega}{\left(\dot{\Omega}\right)^2} = 3$$

- **Surface B field**

$$B_0 = \left(\frac{3Ic^3 P\dot{P}}{2\pi^2 R^6}\right)^{1/2}$$

- **Characteristic age**

$$\tau \approx \frac{-\Omega}{(n-1)\dot{\Omega}} = \frac{P}{2\dot{P}}$$

# Isolated Pulsar P-Pdot Diagram: *Fermi* era

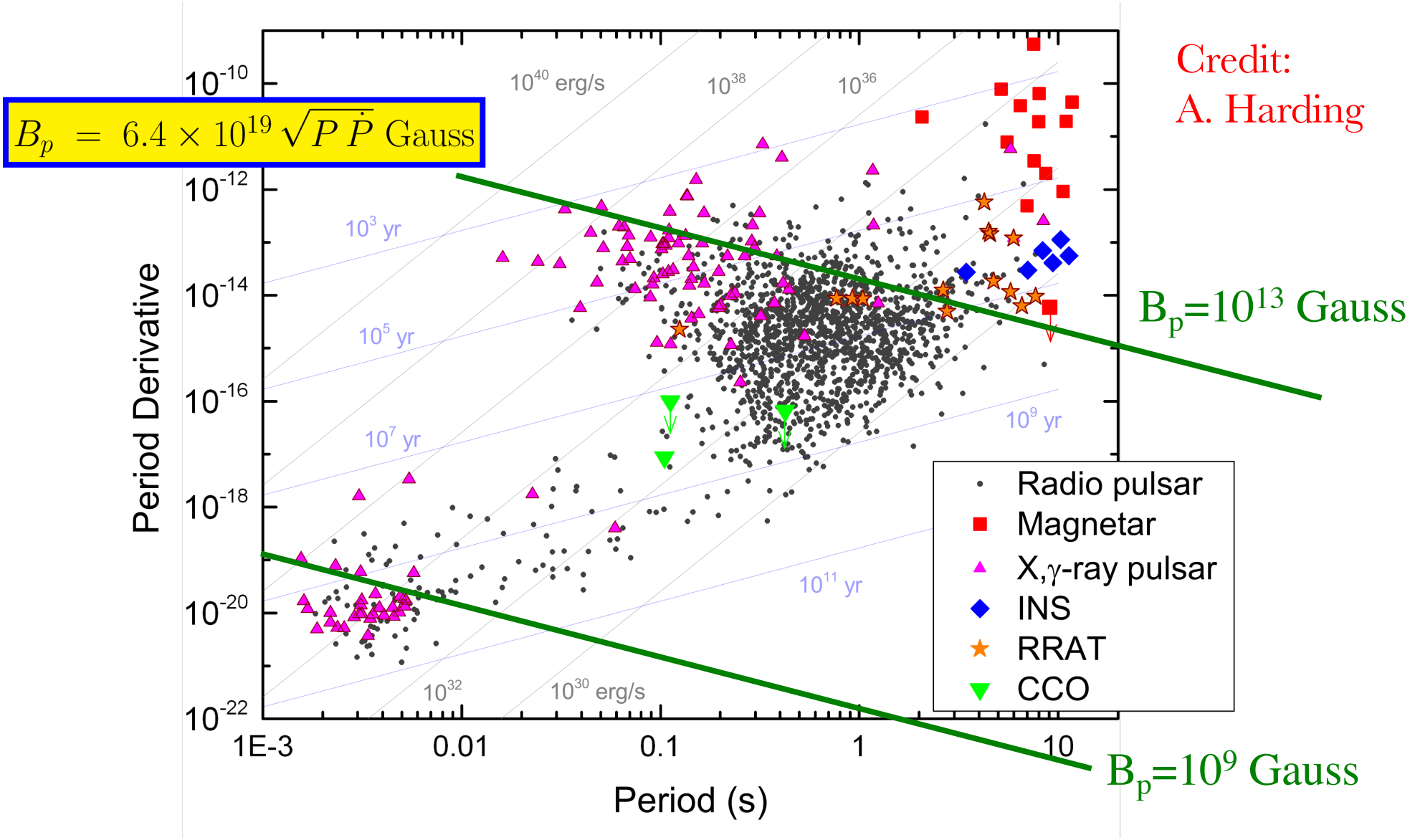


- The phase-space plot for pulsars. Dipole field strength $B_p$ inferences scale as the observable (P Pdot)$^{1/2}$. Nearly 30 magnetars. Many young and millisecond γ-ray pulsars.

# 3 X-ray Pulsars and the Eddington Limit

While radio and gamma-ray emission from pulsars necessarily comes from their magnetospheres, the X-rays mostly come from their stellar surfaces, which are typically at temperatures $T \sim 10^{5.5} - 10^{6.5}\,\mathrm{K}$, with the exception of **magnetars**, which have $T \sim 10^7\,\mathrm{K}$.

• A central question is why do X-ray pulsars never have surface temperatures higher than around $10^7\,\mathrm{K}$ and why do they never have luminosities in excess of $10^{38}\,\mathrm{erg/sec}$? The answer is that for the atmospheric layers to stably exist in the hydrostatic equilibrium, the radiation pressure cannot be too great.

To determine the potential influence of radiation pressure on neutron star atmospheric gas, the starting point is estimating the radiative force per unit volume in the Thomson scattering domain. This is of magnitude

$$|\mathbf{f}| \;\approx\; \frac{n_e \sigma_{\rm T}}{c} \int I_\nu \, d\Omega \, d\nu \quad . \tag{24}$$

This presumes that electrons of number density $n_e$ are the primary targets for radiation scattering with cross section $\sigma_{\rm T} = 8\pi r_0^2/3$. For a spherical star of radius $R$, the integrated intensity can be coupled to the net luminosity to yield a total radiative force on a volume $V = 4\pi R^2 h$ of gas

$$|\mathbf{f}|\, V \;\approx\; \frac{n_e V \sigma_{\rm T}}{c} \, \frac{L}{4\pi R^2} \quad . \tag{25}$$

Let the target gas be of mass $m_g = \rho_g V$, where the mass density of hydrogen gas is given by $\rho_g \approx m_p n_e$ (this can be quickly adjusted to Fe). The gravitational force on the target gas is of magnitude $GMm_g/R^2$. This must bind the gas to the stellar surface and so must be directly compared via an inequality to Eq. (25). In so doing, $n_e$, $R$ and $V$ all cancel when rearranging this inequality, and the result is the luminosity bound

$$L \;\leq\; L_{\rm Edd} \;\equiv\; \frac{4\pi G M m_p c}{\sigma_{\rm T}} \;=\; 1.25 \times 10^{38} \, \frac{M}{M_\odot} \, \mathrm{erg/sec} \quad , \tag{26}$$

the famous **Eddington limit luminosity**. This depends only on the mass of a star, and not on its radius.

• If $L_X$ exceeds $L_{\rm Edd}$, the radiation will blow off the outer layers of the star. Accordingly, stable X-ray emission from the stellar surface must be below this limit. It can in fact exceed the spin-down luminosity, and sometimes does (e.g. magnetars), and may or may not provide a dominant torque on the star that would drive its spin-down.

∗ Employing a Planck spectrum, the fundamental radiation pressure bound $4\pi R^2\sigma T^4 < L_{\rm Edd}$ solves to give $T \lesssim 2\times10^7\,{\rm K}$ (i.e. around 1 keV) for $R = 10^6\,{\rm cm}$ and $M = 1.44M_\odot$. This delivers the essential reason why X-ray pulsar surface temperatures are in the range they are.

• A majority of X-ray pulsars are in compact binary systems, known as **X-ray binaries**, where the neutron star accretes gas from its companion. The infalling gas can set up accretion shocks above the magnetic poles where gas and radiation pressure balance. This sets up a circumstance where higher radiation temperatures are possible in X-ray binaries, and they are generally bright above 10 keV.

**Plot:** X-ray binary accretion geometry

• Accretion onto neutron stars transfers angular momentum to them so as to cause **spin-up** to larger frequencies $\Omega$. This is believed to be the predominant channel for evolution of old pulsars ($> 1\,{\rm Gyr}$) to become fast-spinning **millisecond pulsars**.

# X-ray Binary Accretion Geometry

Schoenherr et al. (2007)

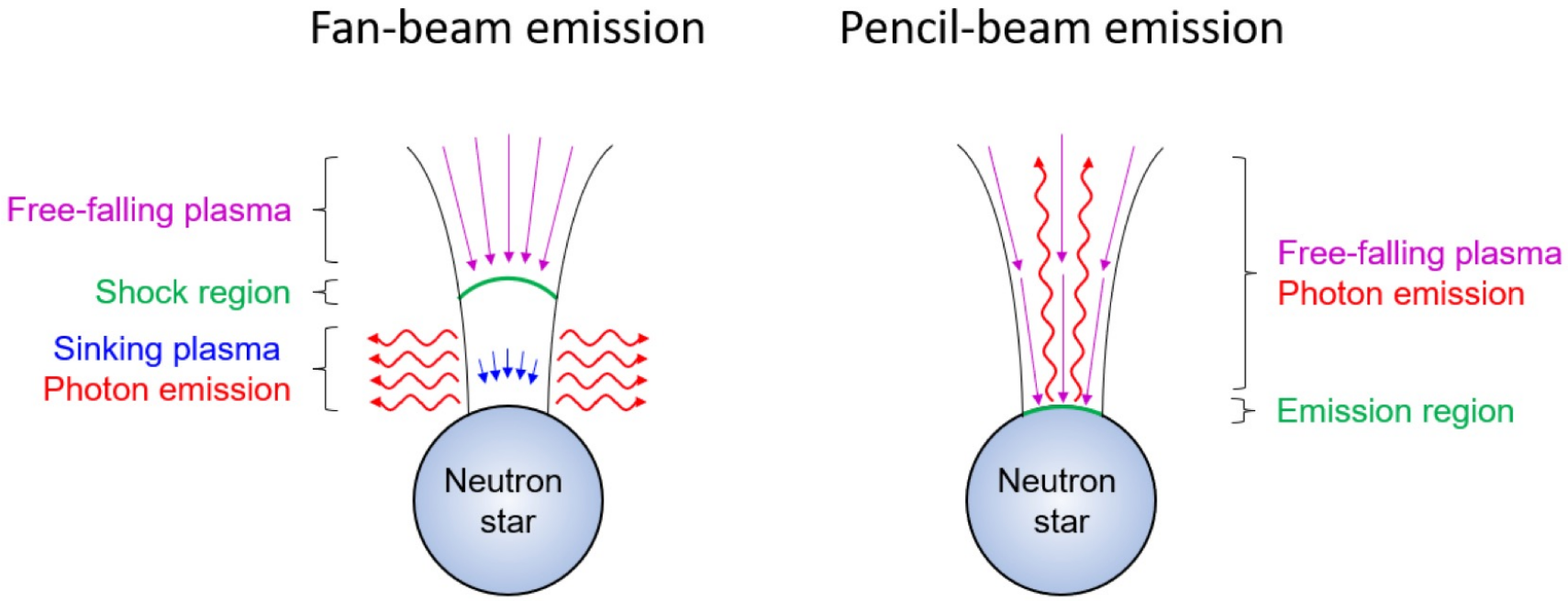


- Two neutron star accretion scenarios, one where intense radiation pressure from the surface stalls accretion inflow to form a shock in the column above the surface (left), and on the right a low radiation case with no stalling.